Decentralized Economic Operation of Isolated AC, DC, and Hybrid Microgrids

Omar M. Abo Gabl¹, Mohammed Y. Morgan², and Mohamed Salah El-Sobki (Jr.)³

1,2,3 Cairo University, Department of Electrical Engineering, Giza, Egypt

omar.abo.gabl@eng.cu.edu.eg, mohammed.yousri1@eng.cu.edu.eg, sobki54-2@hotmail.com

Abstract

In this study, a new economic operation scheme for AC, DC, and hybrid microgrids is proposed using a variable cost-based droop control. The proposed scheme integrates the cost function of the distributed generating units into the primary control level and adjusts the resultant droop characteristics to obtain the secondary control level, thereby eliminating the need for a tertiary control layer. Moreover, a novel DC-normalized cost-based droop is introduced to overcome the voltage drop caused by DC line impedance and to fulfill the economic operation requirements for the DC subgrid. The proposed scheme retains the simplicity and decentralized nature of conventional droop control. The proposed technique employs the Walrus Optimization Algorithm (WaOA) to optimize the resultant droop and is tested on a modified IEEE-38 bus hybrid microgrid to demonstrate the performance of the proposed scheme.

Index-words: Cost-based droop, DC microgrid, Decentralized control, Economic operation, Hybrid microgrid.

I. Introduction

In the last few decades, fossil fuel depletion, in conjunction with increasing demand for electrical energy, has led to the growth of renewable energy technologies [1]. Renewable energy sources (RES) offer clean and sustainable energy. However, replacing traditional energy sources with renewable ones is considered a challenge because of their intermittent and unpredictable nature [2].

Integrating RES into the power system raises some issues for system controllability and stability [3], [4], which highlights the microgrid as a solution to facilitate the integration of RESs into the power system and increase energy efficiency and reliability. A microgrid is defined as a localized group of interconnected loads and sources that function as a single controllable unit and can operate in synchronization with the main grid to permit energy exchange or can operate autonomously according to system operation requirements and conditions. [5], [6]. Microgrids are mainly classified into three types: AC, DC, and hybrid microgrids. In the AC microgrid (ACMG), the whole microgrid is connected to the main grid by an isolation switch, and all AC power sources are connected directly to the microgrid,

while the DC power sources are connected through a DC/AC converter. In the DC microgrid (DCMG), the whole microgrid is connected to the main grid by an AC/DC bidirectional converter, and power sources with DC outputs are coupled to the DC bus directly or via DC/DC converters. Meanwhile, AC/ DC converters are used to connect power sources with AC output to the DC bus. The hybrid microgrid (HMG) merges the AC and DC microgrids using a bidirectional interlinking converter (IC), and the whole microgrid is connected to the main grid by an isolation switch from the ACMG side. Unlike AC and DC microgrids, HMGs support multiple operating modes. HMG can operate in synchronization with the main grid or with the ACMG only while the DCMG is isolated. In the same manner, the AC and DC microgrids can operate isolated together or apart. The combination of AC and DC microgrids into a single hybrid microgrid is introduced in [7], [8]. The foremost benefit of the HMG is having AC and DC common buses, which reduces the required converters and minimizes harmonics as all sources and loads are connected to their relevant bus type, which results in lower investment costs, lower switching losses, lower synchronization issues, and better control [9], [10]. The typical structure of a hybrid microgrid is shown in Fig. 1 [11].

Microgrids have three main control strategies: centralized, distributed, and decentralized control based on the degree of data exchange between involved generation units [12]. Centralized control requires an intricate communication structure and synchronized time frame, while distributed control depends on local controllers with local information exchange with adjacent units. In decentralized control, units can function independently with minimal data exchange utilizing three-level hierarchal control: primary, secondary, and tertiary [13].

Figure 2 outlines the function and response time for each control level. Harmonization of AC and DC microgrids to operate as a unified controllable unit and achieve optimal performance is a critical concern for the HMG's control approach.

Different control strategies and objectives have been used for HMGs to implement economic operations. Loh et al. (2013) and Eajal et al. (2016) conducted the interfacing between AC and DC subgrids by transferring the AC frequency and the DC voltage to a common frame to permit active power exchange [14], [15]. Sun et al. (2020) proposed an energy management system for hybrid microgrids to minimize the operating cost based on day-ahead forecasting of served load using real-time data communication for the neural networks model scheduling. The operating costs include fuel cell, battery, and converter operating and maintenance Abdul-Hamid et al. (2020) utilized the Equilibrium Optimizer Algorithm (EOA) to perform an optimal power flow (OPF) for the economictechnical and

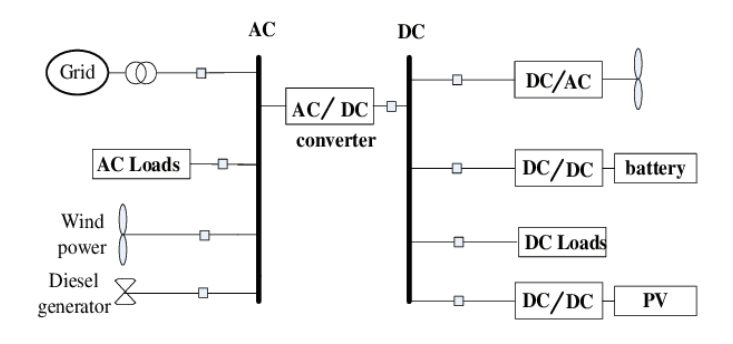


Figure 1: Typical structure of the hybrid microgrid [11].

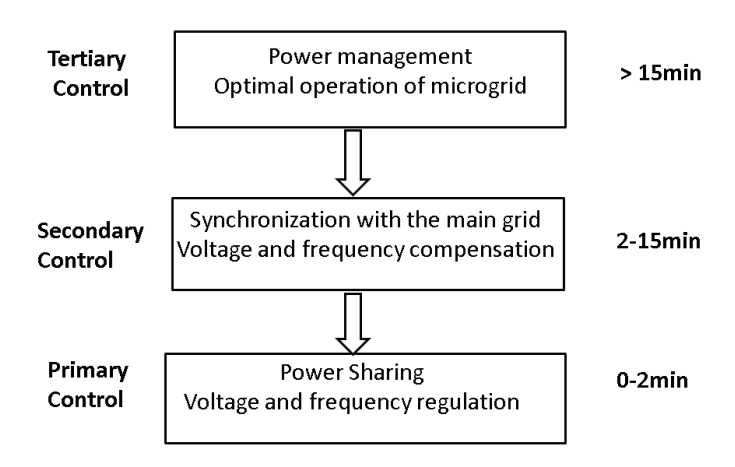


Figure 2: Decentralized hierarchical control levels of a microgrid.

Environmental operation of hybrid microgrids by minimizing the generation cost and emissions along with minimizing the power losses and voltage deviation [17]. An economic operation control strategy is proposed by Yang et al. (2020) for hybrid microgrids based on equal incremental cost for AC and DC microgrids using normalized frequency/DC voltage cost-based droop. However, this approach neglected DC bus voltage deviations caused by DC line impedance. This led to inaccurate DC subgrid generation costs and increased the communication burden to send DC bus voltages to all DGs to form the normalized frequency/DC voltage cost-based droop [18]. Li et al. (2023) and Salman et al. (2024) proposed a global economic operation strategy based on the local economic operation of AC and DC subgrids autonomously, then equalizing the incremental cost for AC and DC subgrids. Parallel interlinking converters are considered, but RES is excluded from the economic operation and treated as a constant output. To ensure equal incremental cost among the AC and the DC subgrids, an economic interaction control is required at the interlinking converters to adjust the power flow through the converters with further communication between converters. Moreover, additional control for DGs in DCMG is required to eliminate the error of voltage deviation caused by line impedance to maintain equal incremental cost [19], [20]. A globally distributed economic operation is proposed by Yang et al. (2025) for multiple AC and DC microgrids. Considering the low X/R ratio and the resistive nature of the lines in

low-voltage microgrids, the proposed control uses a P/V cost-based droop control for the AC and DC microgrids and a consensus algorithm to eliminate the error due to different line impedances to have a unified incremental cost among the microgrids [21].

The contributions of the proposed technique are summarized as follows:

- A variable AC cost-based droop is introduced as a decentralized control strategy for the isolated AC, DC, and hybrid microgrid that reduces the computation and communication burden.
- A novel normalized cost-based droop is introduced in the DC subgrid to perform an economic operation between the RES and overcome DC bus voltage deviation caused by DC line impedance.
- An optimal power routing scheme is proposed

to control the resultant cost-based droop using the Walrus Optimization Algorithm (WaOA) to minimize the ACMG losses and ensure optimal routing of the active power transferred from the DCMG to ACMG.

The rest of the paper is organized as follows. The decentralized economic operation and mathematical formulation are introduced in Section 2. Section 3 defines the mathematical formulation of the optimization problem. Section 4 explains the Walrus Optimization Algorithm (WaOA). The test cases and results are discussed in Section 5. Finally, the conclusion is given in Section 6.

II. Decentralized economic operation strategy

To describe the proposed control technique, the isolated hybrid microgrid IEEE 38-bus system shown in Fig. 3 is considered.

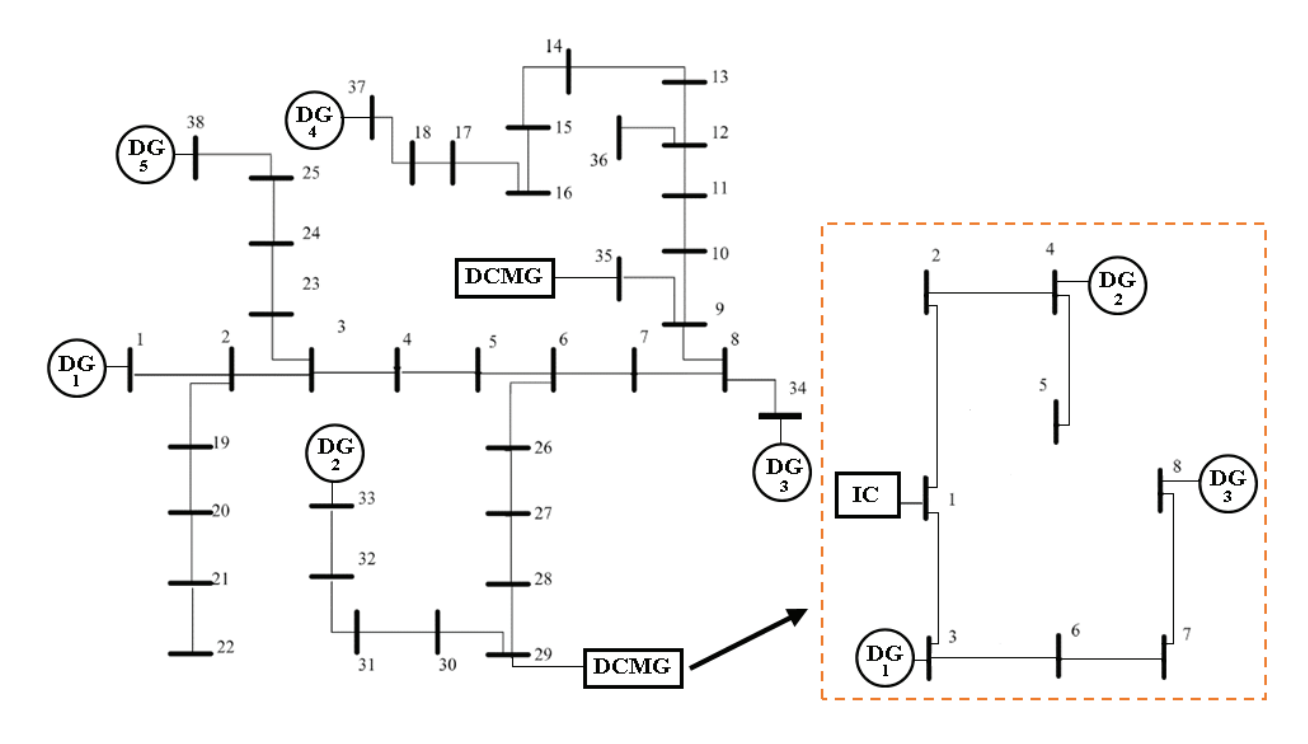


Figure 3: (a) IEEE 38-bus hybrid ac-dc system (b) DC microgrid sub-system.

A. AC microgrid (ACMG)

The cost-based droop presents the most basic economic operation technique for DGs by incorporating the cost function into the droop characteristics and maintaining equal incremental cost at all loading levels [22]. The cost function and incremental cost of the *i*th DG in the AC microgrid (ACMG) are given in Eqs. (1) and (2),

respectively [23]. In order to ensure the minimum cost in the ACMG, the conventional P-f droop is represented by Eqs. (3) and (4), which distributes the power among the DGs according to their ratings (i.e., $P_{DG1,pu} = P_{DG2,pu} = \cdots = P_{DGn,pu}$), is replaced with a cost-based droop that primarily distributes the power according to the operating cost, as defined in Eqs. (5) and (6). In the conventional droop, all DG units use identical droop characteristics, ensuring

equal power sharing among the units, while the costbased droop of each unit varies according to its cost coefficients, with more economical units assigned lower droop values and thus contributing more to power sharing. The cost-based droop is illustrated in Fig. 4.

$$C_i(P_i) = d_i * P_i^2 + e_i * P_i + f_i$$
 (1)

$$\lambda_i = \frac{dC_i(P_i)}{dP_i} = 2d_i * P_i + e_i \tag{2}$$

Where d_i , e_i , and f_i are operating cost coefficients in k^2 , k^2 , k^2 , and k^2 respectively.

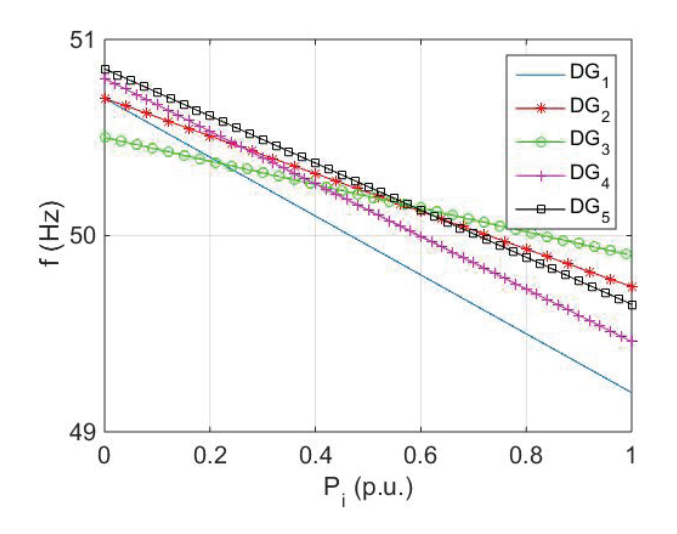


Figure 4: Proposed AC active power cost-based droop.

$$P_{DGi,ac} = \frac{fmax - f}{m_{pi}} \tag{3}$$

$$m_{pi} = \frac{fmax - fmin}{P_{DGi,ac\ max}} \tag{4}$$

$$P_{DGi,ac} = \frac{(fmax - f) - \left(\frac{fmax - fmin}{P_{DGi,ac\,max}}\right) * e_i * h_{ac}}{\overline{m_p}}$$

$$\overline{m_{pi}} = \left(\frac{fmax - fmin}{P_{DGi,ac\,max}}\right) * 2d_i * h_{ac} \tag{6}$$

Where

f: ACMG frequency.

fmax, fmin: Maximum and minimum permissible frequency in ACMG.

 m_{pi} : AC active power droop gain of DG, in ACMG.

 $\overline{m_{pi}}$: AC active power cost-based droop gain of DG_i in ACMG.

 h_{ac} : AC active power droop gain calibration constant.

 $P_{DGi,ac\ max}$: Rated active power of DG, in ACMG.

The reactive power output of DGi in the ACMG is linearly proportional to the bus voltage, as expressed in Eq. (7) and Eq. (8):

$$Q_{DGi,ac} = \frac{Vmax - V_i}{n_{ai}} \tag{7}$$

$$n_q = \frac{Vmax - Vmin}{Q_{DGi,ac\,max}} \tag{8}$$

 V_i : The AC bus voltage of DG_i.

Vmax,Vmin: Maximum and minimum permissible bus voltage in ACMG.

 n_{qi} : Reactive power droop gain of DG_i in ACMG.

 $Q_{DGi,ac\,max}$: Rated reactive power of DG_i in ACMG.

B. DC microgrid (DCMG)

The conventional P-V droop of the DC units is identical, ensuring equal power sharing among the DGs in the DCMG. However, unlike in the ACMG, active power in the DCMGs cannot be shared equally between units due to voltage deviations caused by the impedance of the DC lines. To overcome this voltage deviation and ensure equal incremental cost, a normalized DC cost-based droop is employed. This droop control depends on a common voltage reference shared by the contributing units. The conventional DC P-V droop is replaced by a cost-based droop that distributes the power among the units according to their operating costs. The proposed cost-based P-V droop is illustrated in Fig. 5.

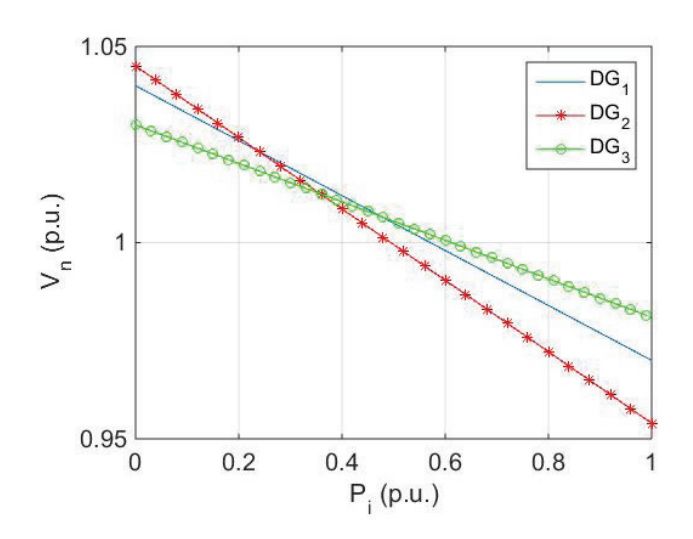


Figure 5: Proposed DC active power cost-based droop.

The DGs in the DCMG are considered to be dispatchable renewable generation coupled with energy storage, and their operating cost can also be modeled as in Eq. (1) [24]. The conventional droop characteristics in Eqs. (9) and (10) are replaced by the cost-based droop defined in Eqs. (11) and (12), and the DGi bus voltage is replaced by the normalized voltage defined in Eq. (13):

$$P_{DGi,dc} = \frac{Vdc, max - Vdci}{m_v} \tag{9}$$

$$m_{vi} = \frac{Vdc, max - Vdc, min}{P_{DG,dc,max}} \tag{10}$$

$$P_{DGi,dc} = \frac{(Vmax - V_n) - \left(\frac{Vmax - Vmin}{P_{DGi,dc \ max}}\right) * e_i * h_{dc}}{m_v} \tag{11}$$

$$\overline{m_{vi}} = \left(\frac{Vmax - Vmin}{P_{DGi,dc\ max}}\right) * 2d_i * h_{dc}$$
 (12)

$$V_n = \frac{\sum_{i=1}^{N_{DG}} P_{DGi,dc \ max} * V_{dci}}{\sum_{i=1}^{N_{DG}} P_{DGi,dc \ max}}$$
(13)

where

Vdci: The DC bus voltage of DG in DCMG.

 V_n : The normalized DC bus voltage.

Vdc, *max*, *Vdc*, *min*: Maximum and minimum DC bus voltage in DCMG.

 m_{vi} : DC active power droop gain of DG in DCMG.

 $\overline{m_{vi}}$: DC active power cost-based droop gain of DG_i in DCMG.

 h_{dc} : DC active power droop gain calibration constant.

 N_{DG} : Number of DGs in DCMG.

 $P_{DGi,dc\ max}$: Rated active power of DG_i in DCMG.

The proposed control strategy block diagrams for the synchronous generator-based DGs and the RESbased DGs are shown in Fig. 6 and Fig. 7, respectively.

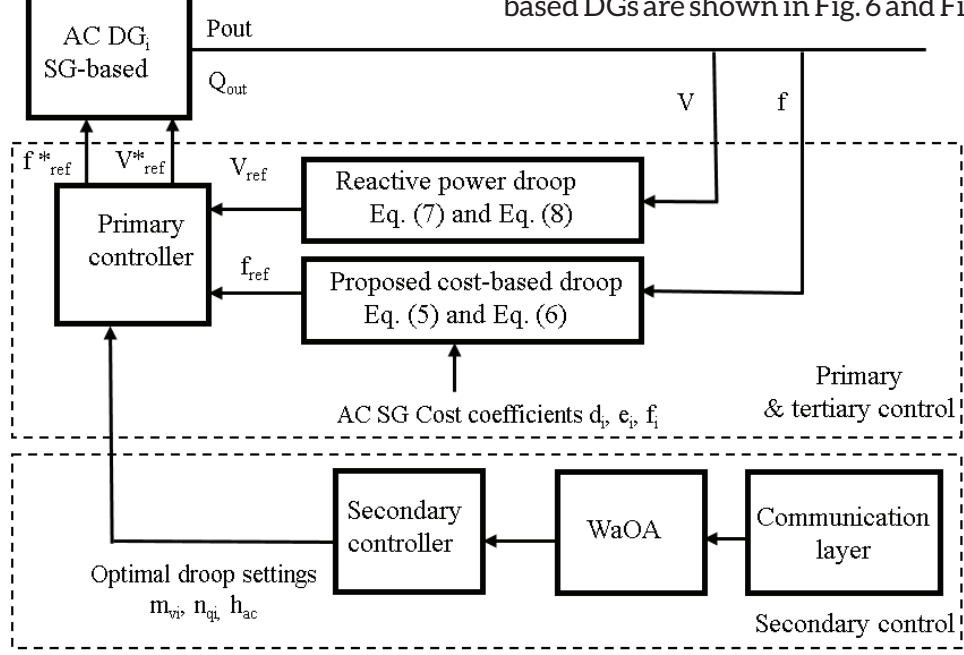


Figure 6: Proposed control strategy block diagram for the SG-based DGs.

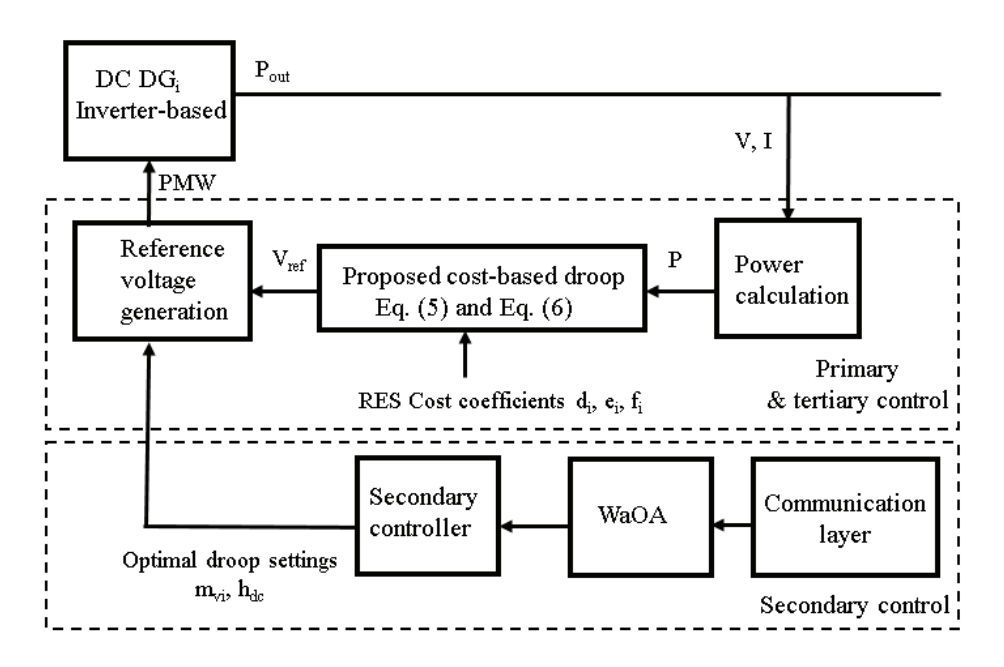


Figure 7: Proposed control strategy block diagram for the RES-based DGs.

C. Interlinking Converter (IC)

The IC is considered a passive gate that permits power to flow in both directions according to the generation in each subgrid. In order to obtain the active power sharing between subgrids, the ACMG frequency and the DCMG IC's bus voltage must be normalized to the same reference frame using Eq. (14) and Eq. (15) [25]. The IC is modeled in the ACMG as a constant active power load or generator depending on the power flow direction, while the power magnitude is obtained from the load flow in the DCMG. The IC incorporates AC reactive power droop, as given in (7) and (8), to support the voltage. In the DCMG, the IC is modeled as a slack bus, and its voltage magnitude is obtained from the ACMG using Eq. (16).

$$f_{norm = \frac{f - 0.5(f_{max} + f_{min})}{0.5(f_{max} - f_{min})}}$$
(14)

$$V_{DC,norm} = \frac{V_{DC} - 0.5(V_{DC \ max} + V_{DC \ min})}{0.5(V_{DC \ max} - V_{DC \ min})}$$
(15)

$$f_{norm} = V_{DC,norm} \tag{16}$$

III. Mathematical formulation

A. Objective function

The optimization objective is to minimize the active power losses in the AC subgrid to further reduce the AC generation cost. The objective function is expressed as shown in Eq. (17). Using the active power losses in the ACMG as an objective function ensures the optimal routing of the active power transferred from the DCMG to the ACMG. The flow chart of the proposed technique is shown in Fig. 8.

$$min \ f(x) = \sum_{i=1}^{Nbr,AC} Ibr_i^2 * R_i$$
 (17)

where

*Ibr*_i: Branch current of line i

 R_i : Resistance of line i

Nbr, AC: Number of branch lines in ACMG

B. Constraints

Power balance:

The power balance constraints ensure that the total generation is equal to the total demand plus losses for the entire hybrid microgrid, and they are represented as follows:

$$\sum_{i=1}^{NDG,ac} P_{DGi,aC} + \sum_{i=1}^{NDG,dc} P_{DGi,dC} = P_{D,aC} + P_{loss,aC} + P_{D,dC} + P_{loss,dC}$$
(18)

$$\sum_{i=1}^{NDG,ac} Q_{DGi,aC} = Q_{D,aC} + Q_{loss,aC}$$
 (19)

where

NDG, ac: Number of DGs in ACMG

 $P_{D,aC}$, $Q_{D,aC}$: Total active and reactive load demand in ACMG

 $P_{loss, ac}$: Total active power losses in ACMG

NDG, dc: Number of DGs in DCMG

 $P_{D,dC}$: Total active load demand in DCMG

 $P_{loss,dC}$: Total active power losses in DCMG

• AC microgrid:

The ACMG constraints include the operational limits of frequency, bus voltage, and DGs ratings, as given below:

$$f_{min} < f < f_{max} \tag{20}$$

$$V_{ac,min} < V_{i,ac} < V_{ac,max} \tag{21}$$

$$P_{DGi,min, aC} < P_{DGi,aC} < P_{DGi,max,aC} \tag{22}$$

$$Q_{DGi,min, aC} < Q_{DGi,aC} < Q_{DGi,max,aC}$$
 (23)

• AC load flow equations:

The conventional load flow equations are formulated as follows:

$$P_{Gi,ac} - P_{Di,ac} - \gamma P_{ICi} = V_i \sum_{j=1}^{Nbus,ac} V_j (G_{ij} \cos \delta ij + B_{ij} \sin \delta_{ij})$$
(24)

$$Q_{Gi,ac} - Q_{Di,ac} + \gamma Q_{Ici} = V_i \sum_{j=1}^{Nbus,ac} V_j (G_{ij} \cos \delta ij - B_{ij} \sin \delta_{ij})$$
(25)

where

$$\gamma = \begin{cases} 1 \text{ if interlinking converter bus,} \\ 0, & \text{otherwise.} \end{cases}$$

 $P_{Gi,ac}$, $Q_{Gi,ac}$: Active and reactive power generated at bus i in ACMG.

 $P_{Di,ac}$, $Q_{Di,ac}$: Active and reactive power demand at bus i in ACMG.

 P_{ICi} , Q_{Ici} : Active and reactive power of the IC at bus i.

 G_{ij} , B_{ij} : Conductance and susceptance of branch between bus i and j.

• DC microgrid:

The DCMG constraints include the operation limits of the bus voltage and DGs ratings, as follows:

$$V_{dc,min} < V_{i,dc} < V_{dc,max} \tag{26}$$

$$P_{DGi,min,dC} < P_{DGi,dC} < P_{DGi,max,dC} \tag{27}$$

• DC load flow equation:

The load flow equation for the DCMG is formulated as follows:

$$P_{Gi,dc} - P_{Di,dc} + \gamma P_{ICi} = V_i \sum_{j=1}^{Nbus,dc} V_j * G_{ij}$$
 (28)

where

$$\gamma = \begin{cases} 1 \text{ if interlinking converter bus,} \\ 0, & \text{otherwise.} \end{cases}$$

 $P_{Gi,dc}$: Active power generated at bus i in DCMG.

 $P_{Di,dc}$: Active power demand at bus i in DCMG.

 G_{ij} : Conductance of branch between bus i and j

Interlinking convert:

Interlinking converter (IC) constraints are represented in the Active and reactive power limits of the converters as follows:

$$P_{ICi,min} < |P_{ICi}| < P_{ICi,max} \tag{29}$$

$$Q_{ICi,min} < Q_{ICi} < Q_{ICi,max} \tag{30}$$

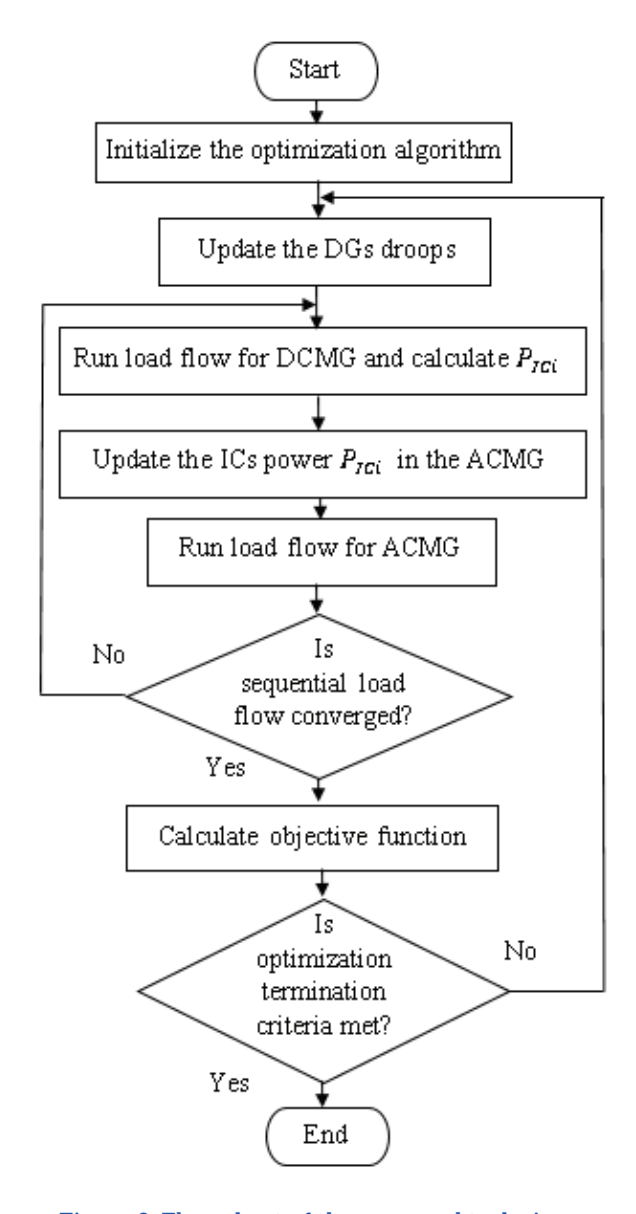


Figure 8: Flow chart of the proposed technique.

IV. Walrus optimization algorithm (WaOA)

The WaOA is used as an optimization technique to control the resultant cost-based droop as a secondary control to minimize ACMG losses. The WaOA originated from the behaviors of walruses. Walruses are considered one of the ocean's largest mammals. Walruses are sociable animals that live in herds. Walruses migrate, reproduce, roost, feed, and escape in response to specific signals (danger and safety signals). The WaOA has two main phases, and it switches between them according to the danger level: the exploration phase (migration) and the exploitation phase (reproduction). During the exploration phase, when the danger signal is high, the walruses change their position to a safer

area. In the exploitation phase, when the danger signal is low, walruses begin to reproduce, roost, and feed [26].

A. Danger signals and safety signals

In each herd, there are one or more walrus guards (vigilantes) who monitor the surroundings, and danger alerts are quickly disseminated if any unforeseen conditions arise. The danger and safety signals in WaOA are described as follows:

$$Danger = A * R \tag{31}$$

$$Safety = r_2 \tag{32}$$

$$A = 2 * \alpha \tag{33}$$

$$R = 2 * r_1 - 1 \tag{34}$$

$$\alpha = 1 - t/T \tag{35}$$

where

 r_1, r_2 : Random variables between [0, 1]

t: The number of iterations.

T: The maximum number of iterations.

B. Migration

When danger signals become significantly high, walrus herds relocate to a more secure environment. During this phase, the walrus position is updated as given below:

$$X_{i,j}^{t+1} = X_{i,j}^t + Migration_step$$
 (36)

$$Migration_step = (X_m^t - X_n^t) * \beta * r_3^2$$
 (37)

$$\beta = 1 - \frac{1}{1 + \exp\left(\frac{t - \left(\frac{T}{2}\right)}{T} * 10\right)}$$
(38)

where

 r_3 : Random variable between [0, 1]

 $X_{i,j}^{t+1}$, $X_{i,j}^{t}$: The new and current position for the ith walrus on the jth dimension

 X_m^t , X_n^t : The current position of vigilantes.

C. Reproduction

Conversely, walrus herds choose to reproduce in their current position when the danger signal is less than one. Throughout the reproduction phase, the two main behaviors are onshore roosting and underwater foraging.

1. Roosting

In this behavior, the position of population members (male, female, and juvenile) is updated. The male position is randomly updated using a Halton sequence. As iterations progress, the female walrus approaches the leader walrus, while juvenile walruses aim to mitigate predators near the outer layers of the population and head to the population's interior, as shown in Fig. 9. The female and juvenile positions are updated as follows:

$$F_{i,j}^{t+1} = F_{i,j}^{t} + \alpha \left(M_{i,j}^{t} - F_{i,j}^{t} \right) + (1 - \alpha) * \left(X_{best}^{t} - F_{i,j}^{t} \right)$$
 (39)

$$J_{i,j}^{t+1} = (X_{best}^t + (LF - 1) * J_{i,j}^t) * P$$
 (40)

where

 $M_{i,j}^{t+1}$, $M_{i,j}^{t}$: The new and current position for the ith male walrus on the jth dimension.

 $F_{i,j}^{t+1}$, $F_{i,j}^{t}$: The new and current position for the ith female walrus on the jth dimension.

 $J_{i,j}^{t+1}$, $J_{i,j}^{t}$: The new and current position for the ith juvenile walrus on the jth dimension

 X_{best}^{t} : The current position of the leader walrus

 LF : Vector of random numbers based on $\mathsf{L\acute{e}vy}$ distribution.

P: Random number of (0, 1).

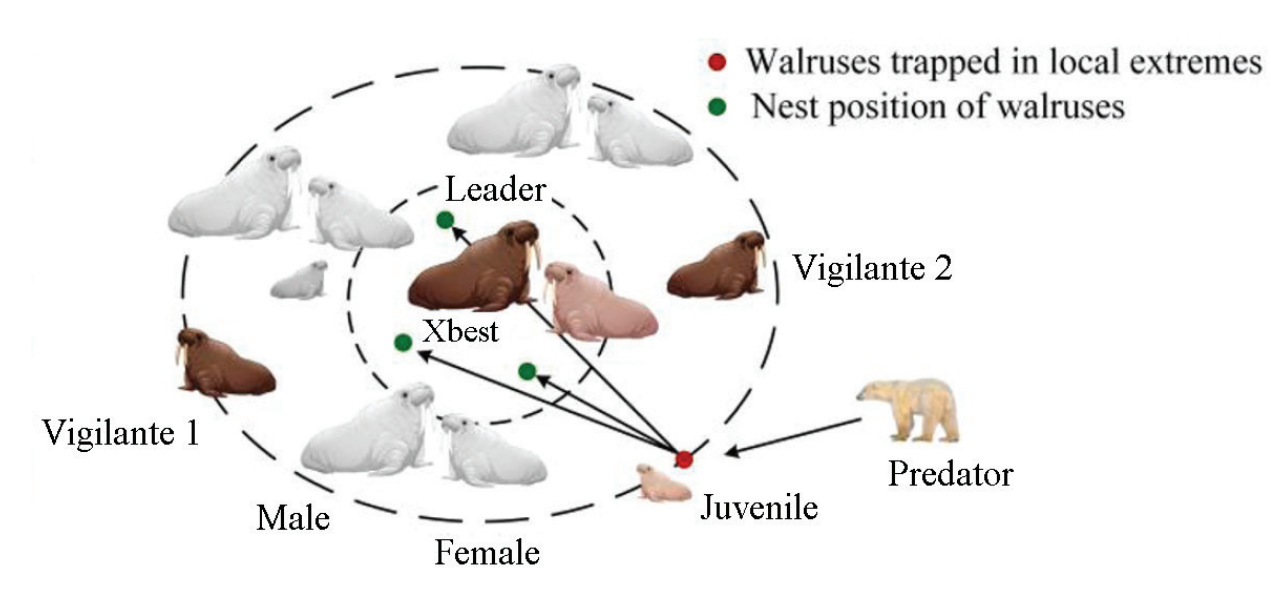


Figure 9: Distribution of walrus herd members in roosting phase [26].

2. Foraging behavior

Underwater foraging is further divided into two behaviors: fleeing and gathering. The behavior selected depends on the level of the danger. When the walruses are attacked by predators, they flee from their position. Otherwise, walruses work together to forage and move according to the location of others in their population. The position updates for fleeing and gathering behaviors are provided in Eq. (41) and Eq. (42).

$$X_{i,j}^{t+1} = X_{i,j}^{t} * R - \left| X_{best}^{t} - X_{i,j}^{t} \right| * r_4^2$$
 (41)

$$X_{i,j}^{t+1} = 0.5(X_{best}^t + X_s^t - \sum_{i=1}^2 a_i b_i +$$

$$\left|X_{best}^{t}-X_{i,j}^{t}\right|+\left|X_{s}^{t}-X_{i,j}^{t}\right|)$$

$$a_{i} = \beta * (r_5 - 1) \tag{43}$$

$$b_{i} = \tan \theta \tag{44}$$

where

r₄, r₅: Random variables between [0, 1].

 X_s^t : The current position of the second walrus in the population.

 θ : Random variables between $[0, \pi]$.

(42) These foraging behaviors, along with other walrus

actions, are modeled in the Walrus Optimization Algorithm (WaOA), which uses danger and safety signals to decide how the population evolves. The integration of these behaviors into walrus optimizer procedure is detailed in the following section.

D. Walrus optimizer procedure

The danger signal in WaOA determines whether the algorithm executes the exploration or exploitation

phase. When the magnitude of the danger signal is greater than one, the herd moves to another solution domain. In contrast, when the danger signal is less than one, the algorithm starts the exploitation phase. The safety signal is important during the exploitation phase because it determines whether individual walruses will roost or forage. Foraging behavior includes gathering and fleeing, depending on the level of danger signals. The full process is illustrated in Fig. 10.

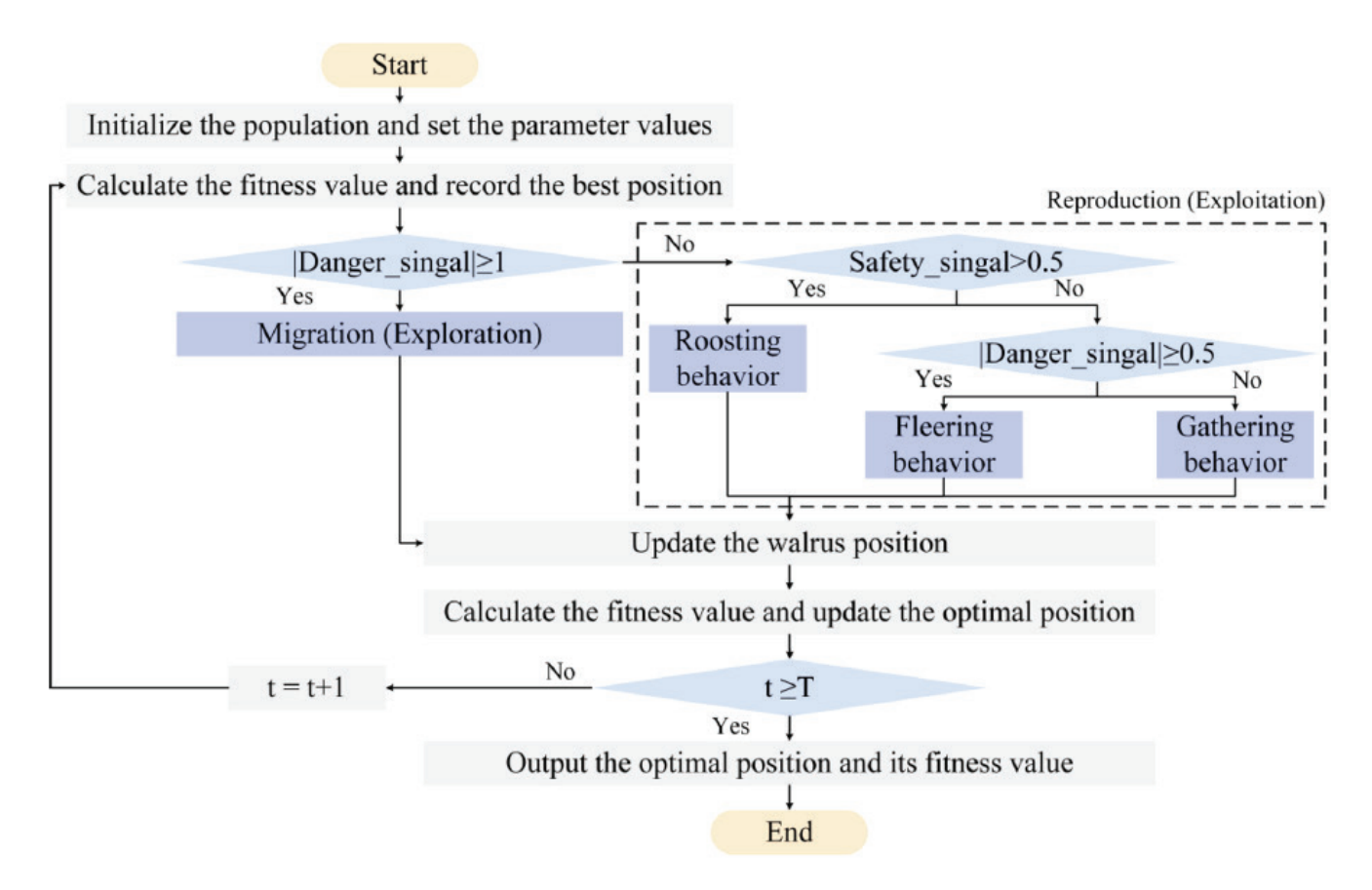


Figure 10: Flow chart of Walrus optimizer procedure [26].

V. Results and Discussions

The proposed approach was tested on the IEEE 38-bus hybrid AC-DC system depicted in Fig. 3. Table 1 contains the DC system's bus and line data, while the generators data of the AC system are given in Table 2, and the rest of the network data is given in [27]. The AC system's base voltage is 12.66 kV, the DC system's base voltage is 0.4 kV, and the hybrid system's base

MVA is 0.01. The interlinking converter power (PIC) is positive when power is transferred from the AC subgrid to the DC subgrid side and negative otherwise. The maximum allowable variance in voltage is ± 0.05 p.u., and frequency is ± 1 Hz. It is important to note that all system equations and the optimization algorithm were formulated and solved within MATLAB using custom script files.

Table 1: Bus and line data for 8-bus DC system

Bus data						Line data			
Bus			P _{G, min}	d	e	f	From	То	R(Ω)
no.	kW	kW	kW	\$/kW²h	\$/kWh	\$/h			
1	10						1	2	0.1
2							1	3	0.2
3		15	2	0.003	0.0306	0.0015	2	4	0.05
4		15	2	0.0045	0.0409	0.0025	4	5	0.02
5	7.3						3	6	0.05
6	7.3						6	7	0.02
8		15	2	0.0019	0.0201	0.001	7	8	0.1

Table 2: Generators data for 38-bus AC system

No.	Bus	P _{max}	P_{min}	Q	d	е	f	
	no.	kW	kW	kVAR	\$/kW²h	\$/kWh	\$/h	
1	1	12	2	9	0.082	4.02	42	
2	33	12	2	9	0.105	2.53	78	
3	34	12	2	9	0.094	1.22	51	
4	37	12	2	9	0.078	3.41	31	
5	38	12	2	9	0.074	3.17	62	
	Interlinking converters							
1	29	12	0	6				
2	35	12	0	6				

In order to validate the proposed technique, three study cases were considered: In case (a), the normalized DC cost-based droop is applied to the isolated DC microgrid presented in Fig. 3 (b), following a fault in the AC microgrid or IC failure causing the DC microgrid to perform autonomously; the result is given in Table 3. Compared with the conventional droop, the proposed approach reduces the total generation cost from 1.5048 \$/h to 1.1337 \$/h by 24.66%.

Table 3: Test results for isolated 8-bus DC system case (a)

Quantity	Before	After
P _{DG1} (kW)	7.84	6.687
P _{DG2} (kW)	9.844	3.314
P _{DG3} (kW)	7.064	13.322
$\lambda_{1}(\$/kwh)$	0.0776	0.0707
λ_2 (\$/ kwh)	0.1295	0.0707
λ_3 (\$/ kwh)	0.0469	0.0707
Total Gen cost (\$/h)	1.5048	1.1337

In case (b), the AC cost-based droop is applied to the isolated AC microgrid only, and the AC active power droop gain calibration constant is controlled to minimize the frequency deviation as in an isolated system with reduced generation, maintaining the system frequency takes precedence over minimizing the system losses. The result is given in Table 4. The proposed droop reduces the total generation cost from 396 \$/h to 382.6 \$/h.

Table 4: Test results for isolated 38-bus AC system case (b)

Quantity	Before	After
f(Hz)	49.7496	50.0682
P _{DG1} (kW)	7.502	2
P _{DG2} (kW)	7.502	8.862
P _{DG3} (kW)	7.502	12
P _{DG4} (kW)	7.502	5.288
P _{DG5} (kW)	7.502	8.25
$\lambda_{1}(\$/kwh)$	5.2504	4.3909
λ_2 (\$/ kwh)	4.1055	4.3909

λ ₃ (\$/ kwh)	2.6305	4.3909
λ_4 (\$/kwh)	4.5804	4.3909
λ_{5} (\$/kwh)	4.2804	4.3909
Total Gen cost (\$/h)	396	382.6

In case (c), the proposed technique is applied on the whole hybrid AC-DC microgrid while the AC active power droop gain calibration constant and the DC droop gains are used as a control variable for the optimization problem given in Eq. (17). It is worth mentioning that in hybrid operation mode, the RES is set to MPPT because their operation cost is considered negligible compared to traditional DGs. The results of case (c) are listed in Table 5; the proposed technique lessens both the total generation cost from 448.2 \$/h to 371.88 \$/h by 17% and the AC active power losses from 0.608 kW to 0.424 kW by 30%. The direction of power flow through the ICs is reversed and goes from the DC microgrid to the AC microgrid. The proposed control strategy reduces AC system losses, minimizes generation costs, and increases the utilization of RES. A comparison of generation costs before and after applying the proposed technique for study cases (a), (b), and (c) is illustrated in Fig. 11.

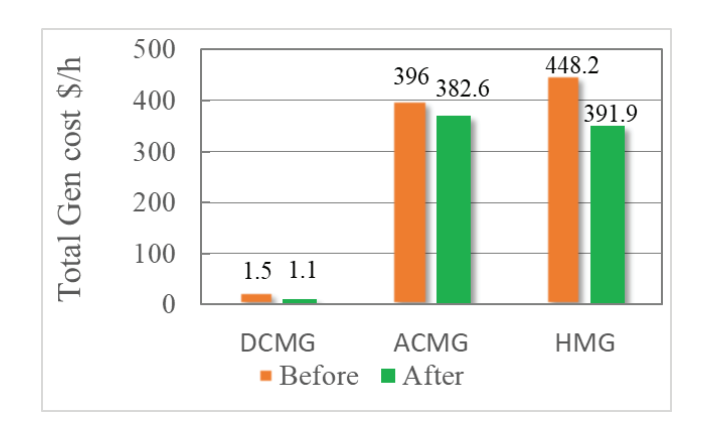


Figure 11: Generation cost comparison of study cases (a), (b), and (c)

In order to validate the optimization technique performance, a comparison study is made between different optimization techniques on the same test system with identical configuration options and population sizes. The compared optimization techniques include Genetic Algorithm (GA) [28], Whale Optimization Algorithm (WOA) [29], Coronavirus Herd Immunity Optimizer (CHIO) [30], and Dandelion Optimizer (DO) [31]. The comparison results are presented in Table 6. The Walrus Optimization Algorithm (WaOA) outperformed the compared algorithms in both objective function and convergence.

Table 5: Test results for 38-bus hybrid AC-DC case (c)

	Quantity	Before		After			
AC microgrid	f(Hz)	49.8136		49.5159	49.5159		
	Pl _{oss} (kW)	0.608		0.424	0.424		
	P _{DGI} (kW)	9.887		2	2		
	$P_{\rm DG2}(kW)$	9.887		7.931	7.931		
	$P_{DG3}(kW)$	9.887		12			
	$P_{DG4}(kW)$	9.887		5.035	5.035		
	$P_{DG5}(kW)$	9.887		6.929	6.929		
	$\lambda_{1}(\$/kwh)$	5.6415		4.348	4.348		
	λ_2 (\$/ kwh)	4.6063		4.1954	4.1954		
	λ_3 (\$/ kwh)	3.0788		3.476	3.476		
	λ_4 (\$/kwh)	4.9524		4.1954	4.1954		
	λ_5 (\$/kwh)	4.6333		4.1954	4.1954		
	Total Gen cost (\$/h)	448.2		371.88	371.88		
ICs	P _{IC} (kW)	5.84	5.84	-2.56	-1.12		
DC microgrids		DCMG1	DCMG2	DCMG1	DCMG2		
	P _{DGI} (kW)	5.99	5.99	8.74	8.28		
	$P_{DG2}(kW)$	7.29	7.29	10.69	10.05		
	P _{DG3} (kW)	5.59	5.59	7.93	7.57		

Table 6: Comparison of optimization techniques applied to the IEEE 38-bus hybrid AC-DC system – case (c) test results

Quantity	GA	WOA	CHIO	DO	WaOA
Pl _{oss} (kW)	0.435	0.4244	0.43432	0.4246	0.424
iterations	30	8	50	12	5

VI. Conclusion

In this study, a decentralized control technique for isolated AC, DC, and hybrid microgrids is presented. The proposed control technique reduces AC active power losses while keeping AC generation costs low. The suggested control strategy aims to maximize the use of renewable energy sources while reducing dependence on traditional fuel-based DGs. The

proposed control approach is simple to develop and implement, and it eliminates the need for tertiary control by integrating the cost function into the primary control drop. Moreover, the new cost-based droops are adjusted using the Walrus Optimization Algorithm (WaOA) to optimize the resultant costbased droop and ensure optimal routing of the active power transferred from the DCMG to ACMG by minimizing the ACMG active power losses. Furthermore, a novel normalized cost-based droop is introduced in the DC subgrid to perform economic operations among the RESs and overcome DC bus voltage deviation caused by DC line impedance. The decentralized nature of the suggested control technique, which is based on local measurements and controllers, improves response time and reliability while reducing system complexity and communication requirements.

References

- [1] H. Hu, N. Xie, D. Fang, and X. Zhang, "The role of renewable energy consumption and commercial services trade in carbon dioxide reduction: Evidence from 25 developing countries," *Appl Energy*, vol. 211, pp. 1229–1244, Feb. 2018, doi: 10.1016/j.apenergy.2017.12.019.
- [2] M. Upasani and S. Patil, "Grid connected solar photovoltaic system with battery storage for energy management," in 2018 2nd International Conference on Inventive Systems and Control (ICISC), IEEE, Jan. 2018, pp. 438–443. doi: 10.1109/ICISC.2018.8399111.
- [3] S. Bouafia and M. Si Abdallah," Numerical study of a solar PV/thermal collector under several conditions in Algeria," *Renewable Energy and Sustainable Development*, vol. 10 no. 2, pp. 233–247, Sep. 2024. doi:10.21622/RESD.2024.10.2.900
- [4] R. T. Moyo, M. Dewa, H. F. M. Romero, V. A. Gómez, J. I. M. Aragonés, and L. Hernández-Callejo, "An adaptive neuro-fuzzy inference scheme for defect detection and classification of solar PV cells," Renewable Energy and Sustainable Development, vol. 10, no. 2, pp. 218–232, 2024. doi: 10.21622/RESD.2024.10.2.929.

- [5] J. M. Guerrero, J. C. Vasquez, and R. Teodorescu, "Hierarchical control of droop-controlled DC and AC microgrids a general approach towards standardization," in 2009 35th Annual Conference of IEEE Industrial Electronics, IEEE, Nov. 2009, pp. 4305–4310. doi: 10.1109/IECON.2009.5414926.
- [6] N. Hatziargyriou, H. Asano, R. Iravani, and C. Marnay, "Microgrids," *IEEE Power and Energy Magazine*, vol. 5, no. 4, pp. 78–94, Jul. 2007, doi: 10.1109/MPAE.2007.376583.
- [7] Peng Wang, L. Goel, Xiong Liu, and Fook Hoong Choo, "Harmonizing AC and DC: A Hybrid AC/DC Future Grid Solution," *IEEE Power and Energy Magazine*, vol. 11, no. 3, pp. 76–83, May 2013, doi: 10.1109/MPE.2013.2245587.
- [8] D. Boroyevich, I. Cvetkovic, R. Burgos, and Dong Dong, "Intergrid: A Future Electronic Energy Network?," *IEEE J Emerg Sel Top Power Electron*, vol. 1, no. 3, pp. 127–138, Sep. 2013, doi: 10.1109/JESTPE.2013.2276937.
- [9] A. Hirsch, Y. Parag, and J. Guerrero, "Microgrids: A review of technologies, key drivers, and outstanding issues," *Renewable and Sustainable Energy Reviews*, vol. 90, pp. 402–411, Jul. 2018, doi: 10.1016/j.rser.2018.03.040.

- [10] A. A. Jabbar, A. Y. Elrayyah, M. Z. C. Wanik, A. P. Sanfilippo, and N. K. Singh, "Development of Hybrid AC/DC Laboratory-scale Smart Microgrid Testbed with Control & Empirical Monitoring System Implementation in LabVIEW," in 2019 IEEE PES GTD Grand International Conference and Exposition Asia (GTD Asia), IEEE, Mar. 2019, pp. 889–894. doi: 10.1109/GTDAsia.2019.8715942.
- [11] L. Jia, Y. Zhu, and Y. Wang, "Architecture design for new AC-DC hybrid micro-grid," in 2015 IEEE First International Conference on DC Microgrids (ICDCM), IEEE, Jun. 2015, pp. 113–118. doi: 10.1109/ICDCM.2015.7152020.
- [12] E. Unamuno and J. A. Barrena, "Hybrid ac/dc microgrids—Part II: Review and classification of control strategies," *Renewable and Sustainable Energy Reviews*, vol. 52, pp. 1123–1134, Dec. 2015, doi: 10.1016/j.rser.2015.07.186.
- [13] A. Bidram and A. Davoudi, "Hierarchical structure of microgrids control system," *IEEE Trans Smart Grid*, vol. 3, no. 4, 2012, doi: 10.1109/TSG.2012.2197425.
- [14] P. C. Loh, D. Li, Y. K. Chai, and F. Blaabjerg, "Autonomous control of interlinking converter with energy storage in hybrid ACDC microgrid," *IEEE Trans Ind Appl*, vol. 49, no. 3, 2013, doi: 10.1109/TIA.2013.2252319.
- [15] A.A.Eajal, E.F.El-Saadany, and K.Ponnambalam, "Equal power sharing in islanded AC/DC hybrid microgrids," in 2016 IEEE Electrical Power and Energy Conference, EPEC 2016, 2016. doi: 10.1109/EPEC.2016.7771682.
- [16] C. Sun, M. Lei, X. Y. Xu, Y. Wang, and W. Dou, "A Hybrid AC/DC Microgrid Energy Management Strategy Based on Neural Network," in Proceedings of the 15th IEEE Conference on Industrial Electronics and Applications, ICIEA 2020, 2020. doi: 10.1109/ICIEA48937.2020.9248228.
- [17] D.T.Abdul-hamied, A.M.Shaheen, W.A.Salem, W. I. Gabr, and R. A. El-sehiemy, "Equilibrium optimizer based multi dimensions operation of hybrid AC/DC grids," Alexandria Engineering Journal, vol. 59, no. 6, 2020, doi: 10.1016/j. aej.2020.08.043.

- [18] P. Yang, M. Yu, Q. Wu, P. Wang, Y. Xia, and W. Wei, "Decentralized Economic Operation Control for Hybrid AC/DC Microgrid," *IEEE Trans Sustain Energy*, vol. 11, no. 3, 2020, doi: 10.1109/TSTE.2019.2946227.
- [19] X. Li et al., "Distributed Unified Control for Global Economic Operation and Resilience Reinforcement of Hybrid AC-DC Microgrids," IEEE Trans Power Electron, vol. 38, no. 7, 2023, doi: 10.1109/TPEL.2023.3259969.
- [20] M. Salman, Y. Li, and J. Xiang, "A Distributed Consensus-Based Optimal Dispatch Control Strategy for Hybrid AC/DC Microgrids," *IEEE Access*, vol. 12, pp. 90997–91010, 2024, doi: 10.1109/ACCESS.2024.3414603.
- [21] F. Yang, Y. Yan, J. Cao, S. Lin, D. Li, and Y. Shen, "Distributed economic operation control in low-voltage resistive hybrid AC/DC microgrid clusters with interlinking converters," *Electric Power Systems Research*, vol. 238, p. 110971, Jan. 2025, doi: 10.1016/j.epsr.2024.110971.
- [22] F. Chen *et al.*, "Cost-Based Droop Schemes for Economic Dispatch in Islanded Microgrids," *IEEE Trans Smart Grid*, vol. 8, no. 1, 2017, doi: 10.1109/TSG.2016.2581488.
- [23] G. Chen, F. L. Lewis, E. N. Feng, and Y. Song, "Distributed Optimal Active Power Control of Multiple Generation Systems," *IEEE Transactions on Industrial Electronics*, vol. 62, no. 11, pp. 7079–7090, Nov. 2015, doi: 10.1109/TIE.2015.2431631.
- [24] I.U. Nutkani, W. Peng, P.C. Loh, and F. Blaabjerg, "Cost-based droop scheme for DC microgrid," in 2014 IEEE Energy Conversion Congress and Exposition (ECCE), IEEE, Sep. 2014, pp. 765–769. doi: 10.1109/ECCE.2014.6953473.
- [25] P. C. Loh, D. Li, Y. K. Chai, and F. Blaabjerg, "Autonomous Control of Interlinking Converter With Energy Storage in Hybrid AC–DC Microgrid," *IEEE Trans Ind Appl*, vol. 49, no. 3, pp. 1374–1382, May 2013, doi: 10.1109/TIA.2013.2252319.
- [26] M. Han, Z. Du, K. F. Yuen, H. Zhu, Y. Li, and Q. Yuan, "Walrus optimizer: A novel natureinspired metaheuristic algorithm," Expert Syst Appl, vol. 239, p. 122413, Apr. 2024, doi: 10.1016/j.eswa.2023.122413.

- [27] D. Singh, R. K. Misra, and D. Singh, "Effect of Load Models in Distributed Generation Planning," *IEEE Transactions on Power Systems*, vol. 22, no. 4, pp. 2204–2212, Nov. 2007, doi: 10.1109/TPWRS.2007.907582.
- [28] M. Mitchell, An Introduction to Genetic Algorithms. The MIT Press, 1996. doi: 10.7551/mitpress/3927.001.0001.
- [29] S. Mirjalili and A. Lewis, "The Whale Optimization Algorithm," *Advances in Engineering Software*, vol. 95, pp. 51–67, May 2016, doi: 10.1016/j.advengsoft.2016.01.008.
- [30] M. A. Al-Betar, Z. A. A. Alyasseri, M. A. Awadallah, and I. Abu Doush, "Coronavirus herd immunity optimizer (CHIO)," *Neural Comput Appl*, vol. 33, no. 10, pp. 5011–5042, May 2021, doi: 10.1007/s00521-020-05296-6.
- [31] S.Zhao, T.Zhang, S.Ma, and M.Chen, "Dandelion Optimizer: A nature-inspired metaheuristic algorithm for engineering applications," *Eng Appl Artif Intell*, vol. 114, p. 105075, Sep. 2022, doi: 10.1016/j.engappai.2022.105075.